ISSN 2321-807X

Investigation of the nanocrystalline SnO_2 Synthesized by Homogeneous Precipitation

M. A. Abdel-Rahim, A. Gaber, A. Y. Abdel-Latief, Mahmoud. N. Abdel-Salam*
Physics Department, Faculty of science, Assiut University, Assiut 71516, EGYPT.
*Corresponding author: E-mail address: m_n_abdelsalam@yahoo.com

Abstract

SnO_2 nanoparticles were synthesized by the homogeneous precipitation method using the reaction of tin tetrachloride pentahydrate and a urea solution has been investigated. The nanocrystalline powder has been traced at different calcination temperatures (300 -1050 ºC), and then characterized by using Thermogravemetric analysis, differential thermal analysis and x-ray diffraction. The microstructure of the obtained nanoparticles has been examined by scanning and high transmission electron microscopy. The average crystallite size, determined by x-ray diffraction, was found to be in the range of 3 – 30 nm. The analysis exhibited a tetragonal phase. Optical properties were investigated by a UV–vis absorption spectrophotometer. The calculated optical band gap lies between 4.47 – 3.71 eV as a result of increasing the calcination temperatures and crystallite size. Surface area and porosity of SnO_2 nanoparticles are measured. Specific surface area is related to pore volume and decreases from 155 m^2/g at 100 ºC to 3.3 m^2/g at 1050 ºC.

Indexing terms/ Keywords: SnO_2 nanocrystalline, homogeneous precipitation, XRD, surface area, optical band gap.

Council for Innovative Research
Peer Review Research Publishing System
Journal: Journal of Advances in Chemistry
Vol. 12, No. 2
editor@cirjac.com
www.cirjac.com

ISSN 2321-807X

Introduction

Nanocrystalline tin dioxide (SnO_2) is an n-type semiconductor with a wide band gap of (3.4-3.8 eV) [1]. In addition, SnO_2 is considered as a stable oxide with good mechanical and chemical properties [1]. Furthermore, SnO_2 nanoparticles have many applications, such as rechargeable Li-Ion batteries [2], heat mirrors [3], transparent electrodes for solar cells [4] and optoelectronic devices [5]. In the field of detection and identification of harmful and toxic gases, tin dioxide semiconductors in the form of thin films or powders are considered as one of the best oxide that can be used for detection of a variety of gases such as hydrogen, carbon monoxide, hydrocarbon, alcohol [6]. Particle size and specific surface area affect of the sensing properties of SnO_2 sensors (sensitivity – selectivity and reproducibility) and these properties can be improved by reducing the particles dimensions [7]. Several methods can be used to fabricate tin dioxide including sol-gel [7], hydrothermal and conventional methods [8], citric acid assisted hydrothermal process [9], solvothermal route [10], amorphous citrate route [6], surfactant mediated [11],mechanochemical processing [12], water –in –oil microemulsions [13] and precipitation method [14, 15]. Homogeneous precipitation method using urea is one of the methods used for preparation of tin dioxide with high surface area and particles in the range of nanometer scale. This can be obtained via controlling in the pH in the solution during decomposition of urea [16, 17].

The advantages of the homogeneous precipitation method lie in the process of controlling the pH through the decomposition of urea as the temperature of the solution is raised to 90 °C. The progressive decomposition of urea leads to increase uniformity and homogeneity in the pH in every part of the solution [16]. Thus, when urea is dissolved into a-homogeneous solution of metal salt, at low temperature urea has a high degree of stability. Furthermore, when the temperature of the solution is kept under 90 °C, urea will decompose slowly and generate ammonia and carbonate in solution gradually and increase the pH under a homogeneous level [18].

The aim of this article is to characterize the nanocrystalline tin dioxide nanoparticles synthesized by the homogeneous precipitation method. The study focused on the effect of the calcination temperature on the crystallite size and activation energy of crystal growth of SnO_2 nanoparticles. The direct optical band gap has been determined. Specific surface area and pore size distribution of SnO_2 nanoparticles calcined at various temperatures have been evaluated by N_2 adsorption using Brunauer, Emmet and Teller (BET); and Barrer, Joiyner and Halenda (BJH) methods.

2. Experimental procedure

2.1. Chemicals

Tin (IV) chloride pentahydrate ($SnCl_4.5H_2O$ 98%) [Stream chemicals USA], Urea ($CO(NH_2)_2$ 99 %) [Loba chemicals India] were used as starting materials. Chemicals used in this study were analytically pure and used without further purification.

2.2. SnO_2 sample preparation

Nanocrystalline tin dioxide (SnO_2) was prepared by the homogeneous precipitation method. (0.9 M) aqueous solution of urea $CO(NH_2)_2$ was added to (0.05 M) aqueous solution of ($SnCl_4.5H_2O$) at room temperature. The mixture was hydrolyzed at 90 ^oC for 4 hours to decompose the urea and a white solution was obtained. The solution was cooled in chilled water (ice and water at equilibrium for 15-20 min), and then separated using a centrifuge operating at 3000 rpm for 20 min. The white gel was washed with deionized water and ethanol several times to remove chlorine ions. The resulting product was dried for 24 h at 100 ^oC in a drying oven, and then ground in a mortar. Finally, the powder was calcined at different temperatures in a muffle furnace for 2 h in the range of 300 – 1050 ^oC.

2.3. Samples characterization

The thermal behavior of the as-dried sample was investigated by simultaneous (TGA) and (DTA) using a SHIMADZU DTA-60H apparatus. The TGA and DTA sample weight was 6.279 mg and was heated at a heating rate of 10 ^oC/min, during non-isothermal heating from room temperature to 750 ^oC. The crystal structure of all samples was characterized at room temperature using a Philips PW1700 X-ray diffractometer (operated at 40 kV and current of 30 mA). Samples were scanned between 20^o and 90^o at a scanning speed of 0.06 ^oC/s using Cu Kα radiation with λ = 1.5418 Å. High resolution transmission electron microscope (HRTEM) and selected area electron diffraction (SAED) were performed using a JEOL JEM-2100 (operating voltage = 200 KV and beam current = 102 μA) were used to examine particle size, phase composition and crystallinity of materials. (SEM) (JEOL JSM-5400 LV) was used to examine the surface morphology and particles shape. An ultraviolet–visible (UV–vis) 2101 PC scanning spectrophotometer in a range of 200 – 900 nm was used to study the optical absorption and the direct optical band gap was determined by analyzing the obtained data. Porosity and specific surface area of SnO_2 nanoparticles calcined at various temperatures were evaluated by N_2 adsorption using Brunauer – Emmet t- Teller (BET) method, using a computer interfaced Nova 3200 series instrument (Quantachrgme, USA), all samples were thoroughly outgased for 3 h at 250 ºC.

ISSN 2321-807X

3. Result and discussion

3.1. Thermal analysis of tin hydroxide

The thermal analysis of the as-dried tin hydroxide was used to determine the optimum calcination temperatures. Fig. 1-a. Shows the TGA curve for $Sn(OH)_4$ in air. The weight loss occurs in three stages I, II and III. The first stage is attributed to the evaporation of physically adsorbed water in the temperature range (22 - 148 ºC). The most weight loss occurs in this stage (~ 9.5 %). This process is confirmed by the endothermic peak at 70 ºC in the DTA thermogram, as shown in Fig. 1-b. The second TGA process in the range (148 – 254 ºC) can be ascribed to the release of the crystalline water (chemically bonded water). The weight loss in this stage is 5.25 %. In contrast, the evaporation of crystalline water seems to be an exothermic process as implied by the DTA exothermic peak which appeared in the DTA thermogram at~ 251 ºC, as shown in Fig. 1-b. This release of heat is coming from the decomposition of the chemical bond. These results are in good agreement with those obtained by Suvacı et al. [17]. The third stage, which appeared above 254 ºC, might be explained by decomposition of ammonia from the powder sample [16, 17]. The total weight loss occurring during the three processes is about 17.5 %. The thermal behavior of powder obtained indicated that the water molecules and hydroxyl group inhibit the growth of particles until the temperature reach to 600 °C that shows a significant increase in particle size [19].

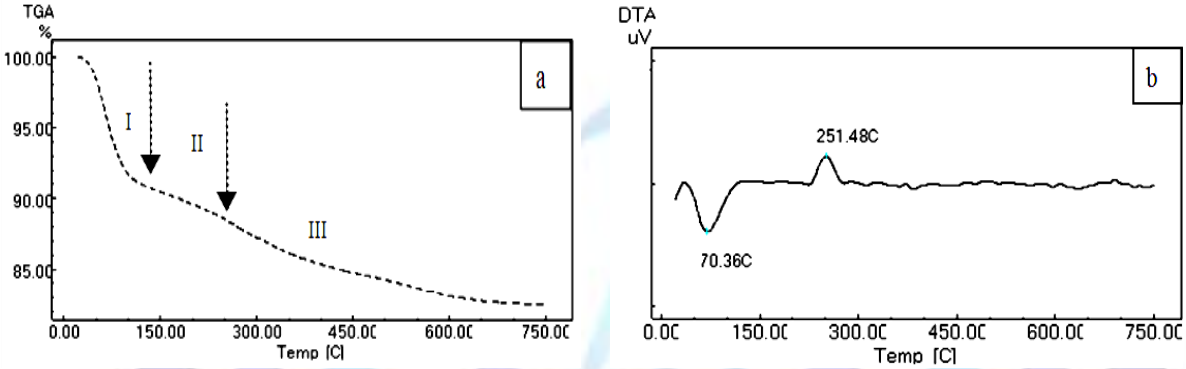

Fig . 1. a) TGA and b) DTA analysis of dried sample.

3.2. Dependence of crystallite size on the calcination temperature

The average crystallite size of tin dioxide nanocrystals was estimated by using the modified Scherrer eq. (1) [10]

$$\mathbf{D = \frac{k\lambda}{\beta \cos\theta}} \qquad (1)$$

Where k is the shape factor 0.89, λ is the X-ray wave length for Cu kα radiation (λ =1.5418 Å), θ is the Bragg diffraction angle (in degrees) and β is the full width at half maximum (FWHM) of the observed peak and corresponding to the instrumental broadening of the standard Si defined as $\beta = (\beta^2_{observed} - \beta^2_{instrumental})^{1/2}$ Fig. 2. Show the XRD patterns of samples calcined at different temperatures. The XRD analysis exhibited that the crystal structure of the fabricated SnO_2 is tetragonal rutile structure with lattice parameters a = b = 4.736 Å and c = 3.185 Å [20]. In the XRD patterns, the broadening of the peaks became narrower with rising the calcination temperature and the crystallinity began above 300 °C. Fig. 3. Describes increases in the crystallite size with increase in the calcination temperature from 450 to 1050 °C. Furthermore, the crystallite size increases steeply and the degree of crystallization does not change after 600 °C. Thus, the temperature does not only effect of the crystallite size, but also the agglomeration of crystallites [17]

ISSN 2321-807X

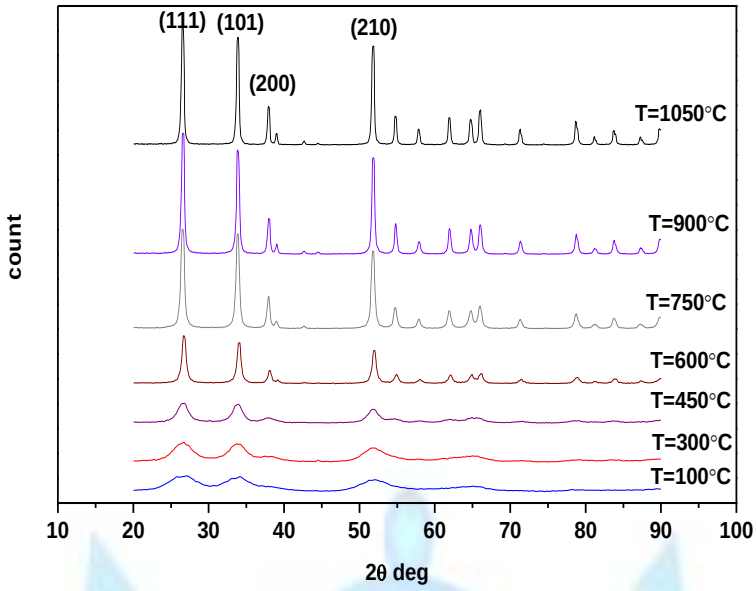

Fig. 2. Shows the XRD charts of the calcined samples at different temperatures.

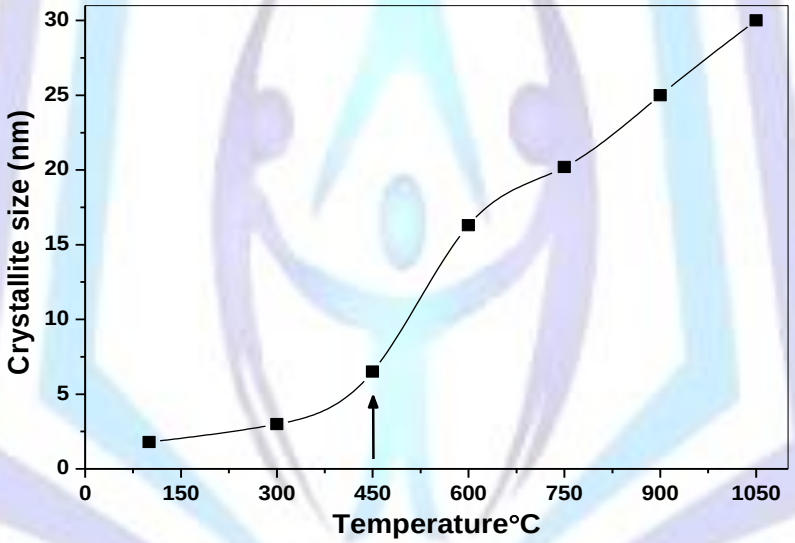

Fig. 3. Dependence of crystallite size with calcination temperature.

The activation energy of crystal growth calculated from the Scott equation (2) describing the process of growth of nanoparticles synthesized by homogeneous precipitation [21]:

$$D = A\, e^{(-E / RT)} \qquad (2)$$

where D is the crystallite size, A is a constant, R is the universal gas constant, T is the absolute temperature and E is the activation energy for the growth of nanoparticles which determined from the slope of the straight line ln(D) versus 1/T as shown in Fig. 4. Under the condition of homogeneous growth of crystals with increasing the calcination temperature in the range from T = 600 to 1050 °C. The calculated activation energy is equal to E = 13.05 kJ/mol. This value is, comparable of the previous work [14], implies that the driving force for the growth of nanoparticles is low and the crystallite growth by interfacial reaction [22, 23].

ISSN 2321-807X

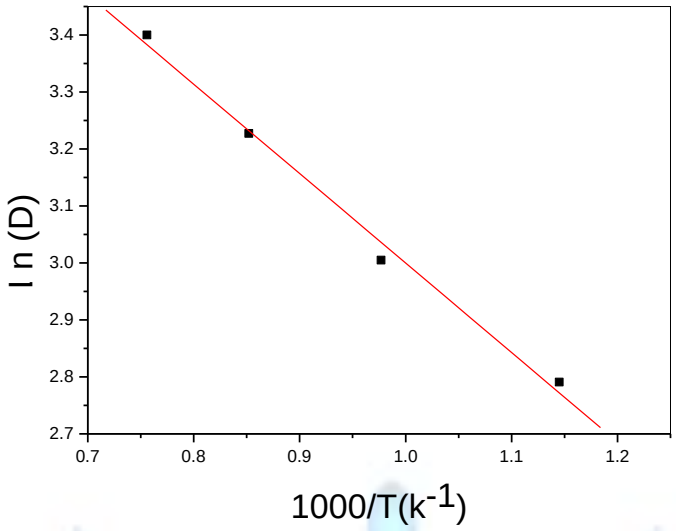

Fig. 4. Determenation of activation energy by plotting ln(D) vs. 1/ T.

3.3. HRTEM and SEM of SnO_2 nanoparticles

The micro - structure of the SnO_2 samples calcined at T = 450, 600, and 750 ºC, are shown in the HRTEM micrographs in Fig. 5. The SnO_2 crystals that calcined at 450 ºC for 2 h show a mesostructure which is looking like a network with spherical (balls) nanoparticles connected to each other in chains. This result is exactly similar to that obtained by Baik et al. for SnO_2 heat treated at 120 ºC for 24 h [24]. On the other hand, the nanoparticles seem to appear as spheres as the calcination temperature rises to 600 and 750 ºC. The average particle size increases as a function of temperature with the average diameter equal to 7.6, 17 and 27.7 nm for T = 450, 600 and 750 ºC, respectively. The HRTEM results confirm the XRD results giving that the nanoparticle size is dependent on the calcination temperature. These results are in fair agreement with the crystallite size determined by XRD line broadening. It is clearly that the SnO_2 nanoparticles have a heterogeneous distribution and the shapes of particles are similar. As the calcination temperature increases the degree of agglomeration of particles become denser. The selected area electron diffraction (SAED) pattern images of SnO_2 nanoparticles are characterized by diffraction rings with discrete spots which indicate that tin dioxide is fully crystalline and the results are in good agreement with the XRD patterns. The lattice spacing that determined using HRTEM are 0.28, 0.35 and 0.44 nm for samples calcinated at 450, 600 and 750 ^{o}C, respectively. The interplanar spacing appeared in the HRTEM micrographs are different from XRD due to different orientation of imaged crystals.

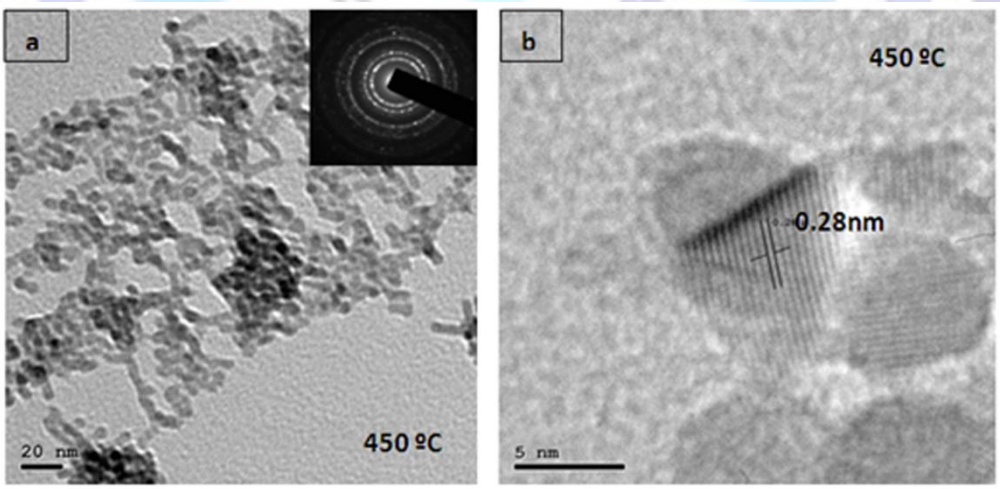

ISSN 2321-807X

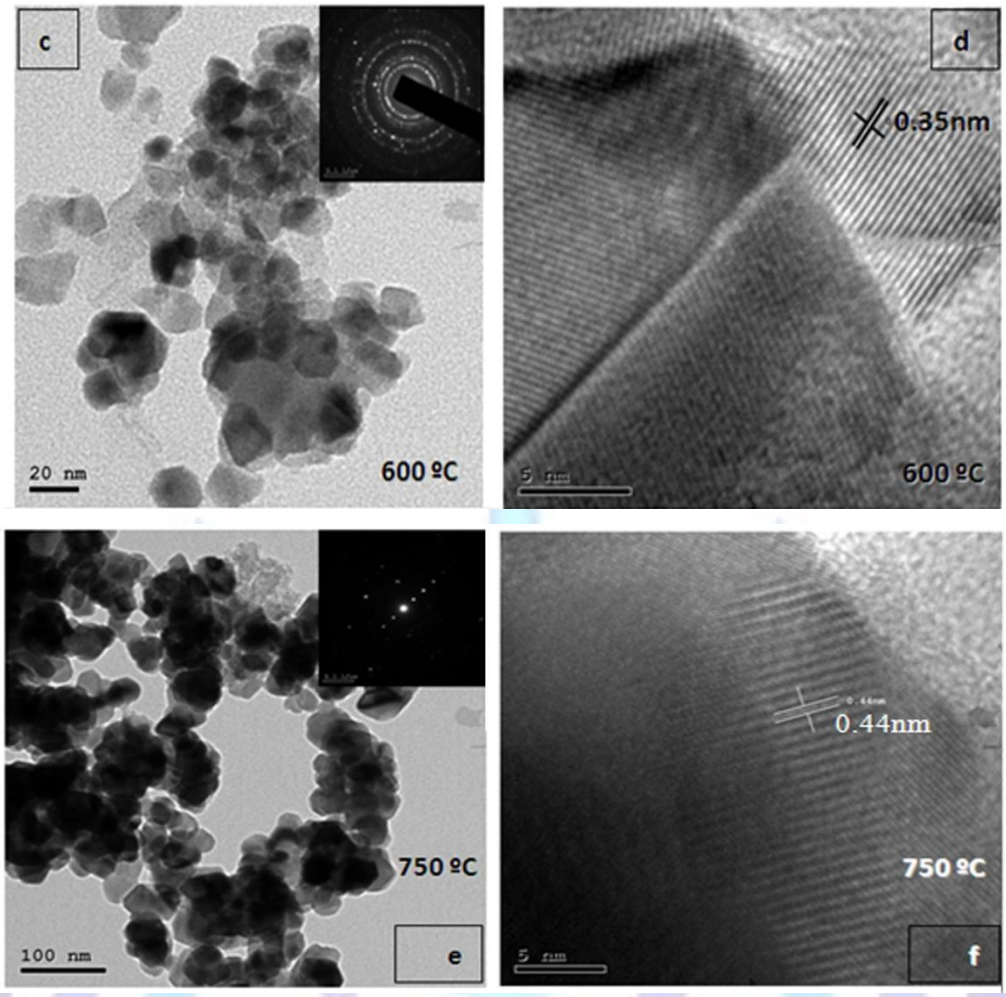

Fig . 5. HRTEM images and SAED of SnO_2 nanocrystals calcined at different temperatures a, b) T = 450 ºC, c, d) T = 600 ºC, e, f) T = 750 ºC respectively.

The SEM micrographs of the as - prepared powder and samples calciend at 750, 900 and 1050 °C are shown in Fig. 6. All images illustrate the impact of the regular decomposition process of urea at 90 ºC during preparation of tin dioxide nanocrystals. When urea decomposes, it generates hydroxide ions which lead to precipitation of the metal oxide or hydroxide [25]. The as-prepared powder Fig. 6-a. dried at 100 ºC has low size distribution with non- uniformed size of particles. Fig. 6-b. shows the morphological image of SnO_2 sample calciend at 750 ºC. It reveals that irregularly sized and arranged in a random manner compact grains with sponge like structure. Spongy cap of large - grained are overgrown on smaller grains [26]. For samples calcined at 900 and 1050 °C in Fig. 6-c, d. the particles become denser with non-uniformly distributed various sized in the sample calcined at 900 °C. But the samples calcined at 1050 °C have a compact arrangement of uniform size particles. From these observations it is seen that the average particle size of samples depends on the calcination temperature and increases with increasing in the calcination temperature. Furthermore, the degree of crystallization increases with increasing the calcination temperature. This result indicates that the SnO_2 samples are useful in gas sensing application by increasing in sensing efficiency as a function of temperature.

ISSN 2321-807X

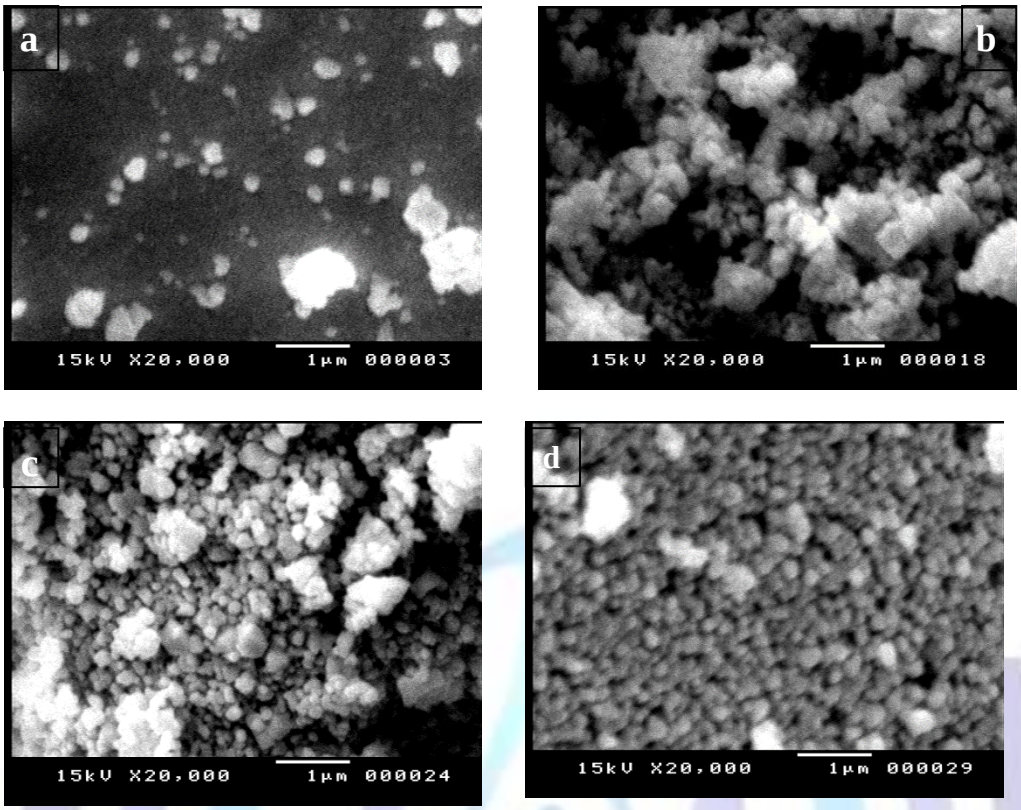

Fig. 6. SEM micrographs of the surface of SnO_2 nanocrystals at different temperatures a) as prepared powder, b) T = 750 ºC, c) T = 900 ºC and d) T = 1050 ºC respectively.

3.4. Optical properties

The optical samples of SnO_2 nanoparticles are synthesized as the same in the previous work [15]. Fig.7. describes typical optical absorption spectra for samples B2, B3, B4 and B6 that calcined at 300, 450, 600 and 900 °C, respectively. The sharp spectrum with high absorbance in the UV-Vis region can be related to a stable nanosuspension solution containing highly crystallized SnO_2 nanoparticles. Furthermore, the absorption edges for all samples are shifted to shorter wave length (blue shift) which indicate higher optical band gap than the reported value of the bulk SnO_2 (3.6 eV) [27]. And the absorbance of samples decreases with increase in the calcination temperature. The direct optical band gap in a semiconductor is determined by assuming the nature of the transition (r) and plotting $(\alpha h\upsilon)^{1/r}$ vs. (hυ) using Eq. (3)[15], where r represents the nature of the transition. In this case (r = 1/2) for direct allowed transition.

$$\alpha h\upsilon = B\,(h\upsilon - E_g)^n \qquad (3)$$

Fig.8. shows plotting $(\alpha h\upsilon)^2$ vs. (hυ) for the samples. The values of E_g obtained from the extrapolation of the linear portion of the curve $(\alpha h\upsilon)^2$ to hυ = 0 in the high energy region of the absorption edge. The direct optical band gap energy, decreases from 4.47 to 3.71 eV with increase in crystallite size from 3 to 25 nm, exhibit an almost 0.11 eV blue shift from that of the bulk value of SnO_2 [1, 27]. In addition, the determined values of optical band gap are comparable with the band gap calculated in literature [15, 28]. When the particle size decreases the band gap increases and this can be attributed to the quantum size confinement effects of SnO_2 nanoparticles [28, 29]. The quantum size confinement effects are expected for semi-conducting nanoparticles and the band gap becomes larger with decreasing particle size, and is indicated by an absorption shift to higher energy. The levels of the valence band are moderately shifted to lower energies, while those of the conduction band are strongly shifted to higher energies [28, 30].

ISSN 2321-807X

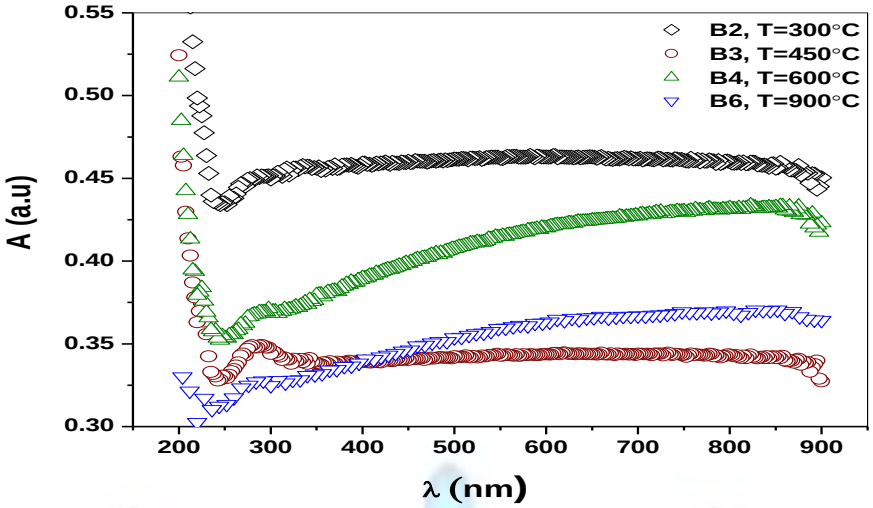

Fig. 7. UV–vis absorption spectra for all SnO_2 samples calcined at indicated temperatures.

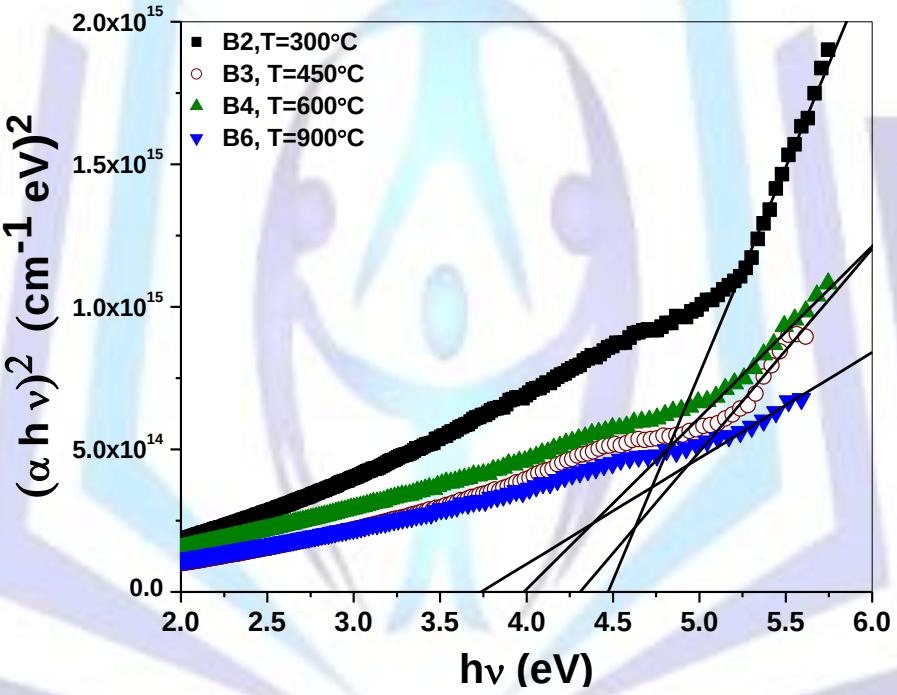

Fig. 8. Plots of $(\alpha hu)^2$ vs. photon energy for SnO_2 nanoparticles calcined at 300, 450, 600 and 900 ^oC.

3.5. Surface area and porosity of tin dioxide (SnO_2) nanoparticles

N_2 adsorption / desorption technique was used to indicate the surface area and porosity of tin dioxide nanoparticles synthesized by homogeneous precipitation method. Fig.9. shows the isothermal curves for dried samples and samples calcined in the temperature range 300 – 1050 ˚C. In the dried sample B1 and sample B2 that calcined at 300 ˚C, the curves illustrate that the samples show similar type I adsorption isotherm behaviors with H4 type of hystersis loops according to the IUPAC classifications [26, 31]. This type of adsorption isotherm related to microporous solidsand the hysteresis loop is often associated with narrow slits like pores as a result of agglomerates or aggregates of particles forming slit pores with uniform size and shape [26, 32]. On the other hand, the samples from B3 to B7 that calcined at temperatures range from 450 to 1050 ˚C, respectively, the isothermal curves of these samples are corresponding to typical type II isotherm. These isotherms indicate that the samples are non- porous or macroporous solids with a high energy of adsorption. In addition, the hysteresis loops for these samples are H4 which means that the material is often associated with narrow slit- like pores as in the previous two samples B1, B2. The N_2 adsorption amounts are decreased with increasing the calcination temperature which indicates decrease in specific surface area of the samples.

ISSN 2321-807X

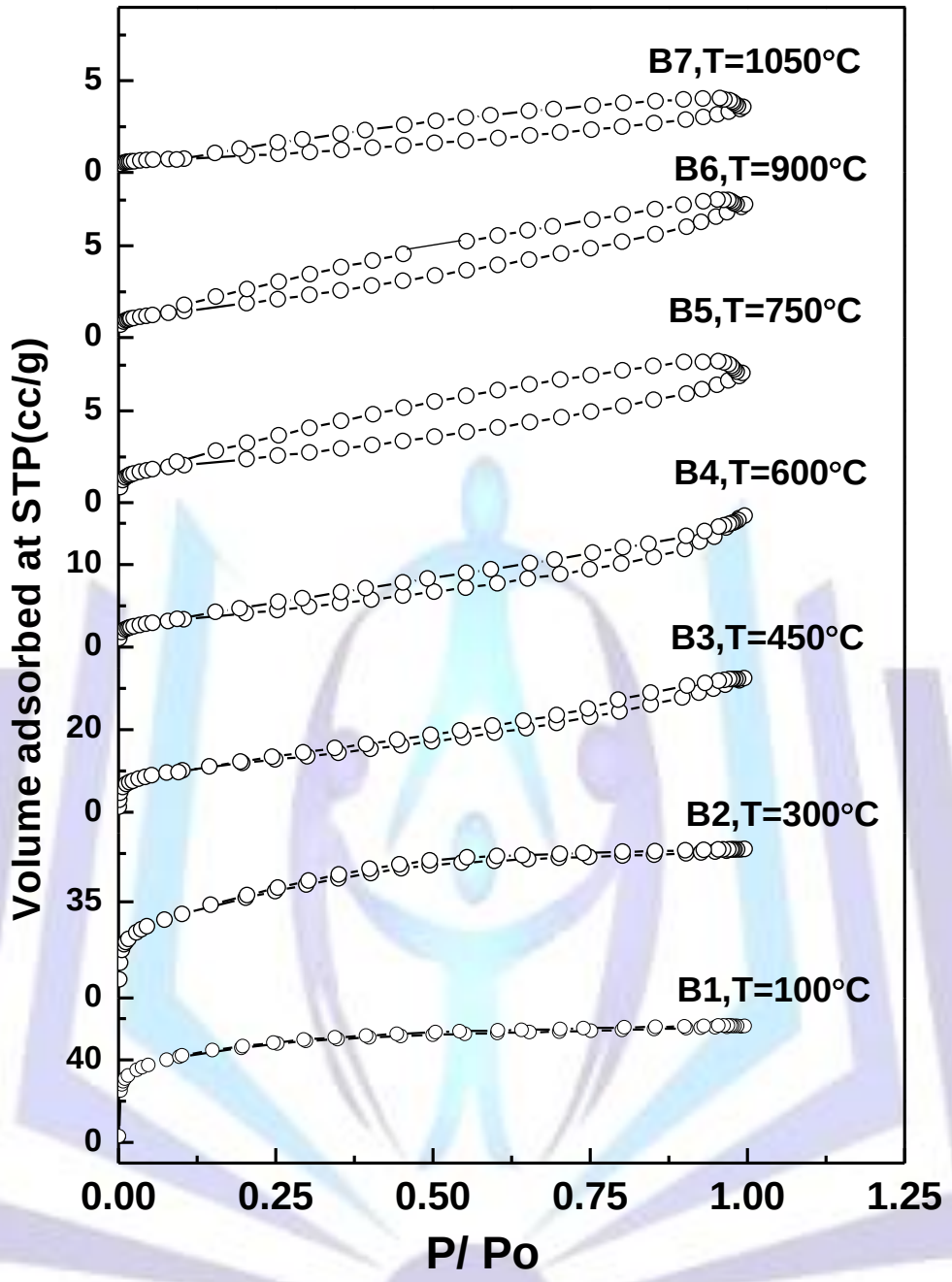

Fig.9. Nitrogen adsorption / desorption isotherms for the SnO_2 nanoparticles calcined for 2 h at different temperatures.

Plot of specific surface area of the powders calcined at different temperatures and total pore volume is illustrated in Fig. 10. It isobserved that the pore volume and specific surface area are decreasing with increasing the calcination temperature due to the increase in the particle size and degree of agglomeration by the effect of sintering occurring in the materials. The specific surface area decreases sharply from 127.7 m^2/g at 300 ˚C to 42 m^2/g at 450 ˚C. The high surface area of SnO_2 at low calcination temperature suggests the small size of particles, afterward the surface area decreases slowly when the particles increase after calcination temperature increase from 600 to 1050 ˚C. The sharp decrease in the surface area can be caused by elimination of ammonia that generated by decomposition of urea, physical and chemical bonded water during transformation of tin hydroxide to pure tin dioxide nanoparticles that allowing the particles to assemble and thus greatly diminished in the surface area [33]. This result indicates that the specific surface area is related to the drop in the total pore volume. By assuming that the particles are spherical shaped and uniform size, the average particle size can be estimated from Brunauer, Emmet and Teller (BET) equation (4) [7].

$$D = \frac{6000}{\rho A} \qquad (4)$$

ISSN 2321-807X

where D is the average particle size in nm, **ρ** is the theoretical density of tin dioxide nanoparticles (6.95 gm/cm^3) and A is the specific surface area at indicated temperature in m^2/g.

Fig.11. determine the difference between the average crystallite size estimated by XRD and the average particle size estimated by BET. The results are consistent only at the low temperatures due to high surface area and smaller particle size. But in contrary, at high temperature the average particle size calculated by BET is significantly larger than the crystallite size calculated by XRD which is attributed to the aggregates or agglomerate of crystals with increasing the calcination temperature. Condense of the surface group in the SnO_2 lattice leads to sharply decrease in the surface area. This result suggests that, the particle size contain several crystals [34]. It can be concluded that the temperature is the main factor affects on the surface area, pore size distributions and particle size of SnO_2 nanoparticles.

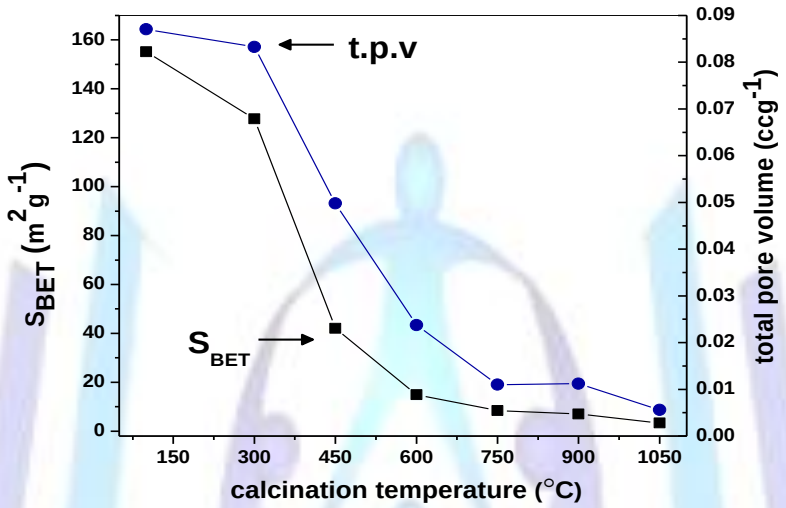

Fig. 10. Variations of specific surface area and total pore volume as a function of the calcination temperature of SnO_2 nanoparticles.

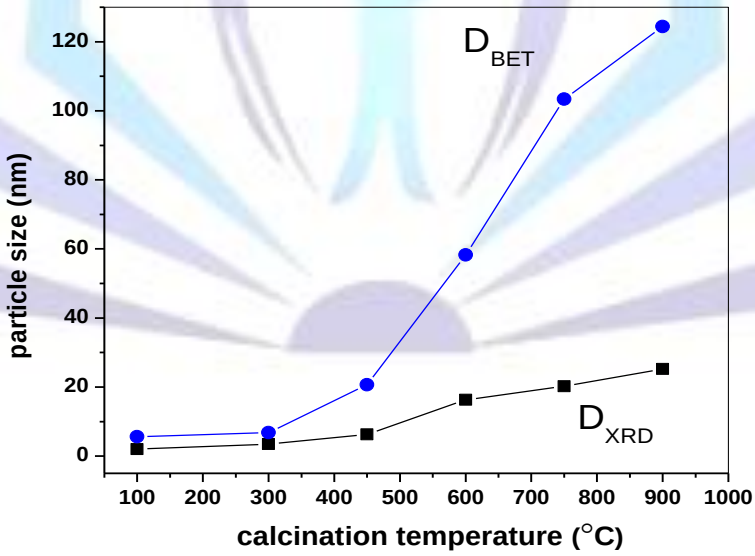

Fig. 11. Variations of crystallite size calculated from XRD and particle size calculated from BET of the SnO_2 as a function of calcination temperature.

Pore size distribution of the samples calcined at various temperatures obtained by BJH method is illustrated in Fig.12. The mean peaks of all samples are in the range between 2 to 4.4 nm. But the sample B3 have two peaks one centered at 4.4 nm and another peak centered at 9 nm. These peaks indicate that the pore size distributions are very narrow with micropores and mesopores in samples. On the other hand, some weak and wide peaks appear in the samples B5 and B7 in the range between 82 nm and 88 nm that indicating macroporous structure of the oxide. Pore volume decreases with

ISSN 2321-807X

increasing in the calcination temperature. But in contrast, the average pore diameters are increasing with increasing the calcination temperature. The increase in the average pore diameter caused by agglomeration of particles that lead to sintering of pores to small pores and decreasing in the homogeneity of the pore dimensions [19]. Table 1 gives the relation between surface area, total pore volume and average pore diameter of SnO_2 nanoparticles with calcination temperature.

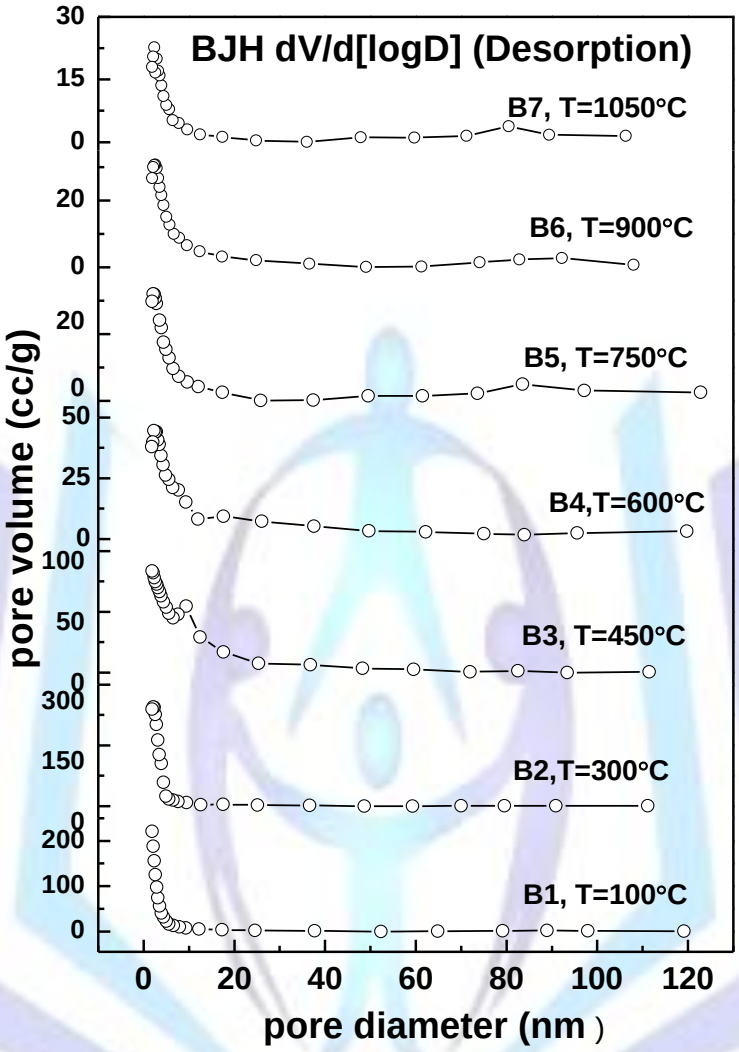

Fig. 12. pore- size distributions of SnO_2 samples calcined at indicating temperature.

Table1: Specific surface area, porosity and particle size of the SnO_2 nanoparticles.

Temperature (˚C)	Specific surface area(m^2/g)	Average pore diameter(nm)	total pore volume (cc/g)	Particle size by BET (nm)
100	155.13	2.2451	0.087	5.6
300	127.72	2.6078	0.083	6.8
450	42.02	4.7377	0.050	20.7
600	14.93	6.3642	0.024	58.2
750	8.41	5.2342	0.011	103.4
900	6.99	6.3968	0.011	124.4
1050	3.33	6.7192	0.006	257.4

ISSN 2321-807X

4- Conclusions

From investigation of SnO_2 nanoparticles synthesized by homogeneous precipitation method the following conclusions can be drawn:

i) The crystallite size of the nanoparticles increases as the calcination temperature increases, i.e. the crystallite size is temperature dependent.

ii) The activation energy of the crystallite growth (13.05 kJ/mole) is rather law which means that the driving force for the growth is relatively low.

iii) The HRTEM examinations show mesostructure of nanoparticles and nanoballs shape.

iv) The SEM examinations revealed that as the calcination temperature increases, the decomposition of particles into smaller and denser spherical particles has taken place. This result implies that the micropores density of the particles increases. This will increase the efficiency of SnO_2 sensing.

v) The direct optical band gap of calcined nanoparticles was found to decrease with the increase in crystallite size.

vi) Specific surface area of SnO_2 nanoparticles lies in the range 155.13 m^2/g to 3.33 m^2/g as the temperature rises from 100 to 1050 ˚C. Decreasing in the surface area is related to sintering of pores to small pores which lead to decrease the number of pores.

vii) Pore size distributions measured by BJH indicate that the nature of pores in SnO_2 nanoparticles is collections of micropores with little mesopores.

References

[1] Bagheri-Mohagheghi, M. M., Shahtahmasebi, N., Alinejada, M. R., Youssefi, A., and Shokooh-Saremi, M., (2008) The effect of the post-annealing temperature on the nano-structure and energy band gap of SnO_2 semiconducting oxide nano-particles synthesized by polymerizing–complexing sol–gel method, Physica B, 403 (13), 2431-2436.

[2] Park, M.S., Wang, G.X., Kang, Y.M., Wexler, D., Dou, S.X., and Liu, H.K. (2007) Preparation and electrochemical properties of SnO_2 nanowires for application in lithium-ion batteries, Angew. Chem. Int. Ed, 46 (5), 750-753.

[3] Hirunlabh, J.,Suthateerane, S., Kirtikara, K., and Pynn, R.D. (1998) Development of a Spray Pyrolysis Coating Process for Tin Oxide Film Heat Mirrors, Thammasat Int. J. Sc. Tech., 3(2), 10-20.

[4] Hau, S.K., Yip, H.L., Zou, J., and Jen, A.K.Y. (2009) Indium tin oxide-free semi-transparent inverted polymer solar cells using conducting polymer as both bottom and top electrodes, Organic Electronics, 10, 1401-1407.

[5] Kim, T.W., Lee, D.U., Choo, D.C., Kim, J.H., Jeong, H.J., Jung, M., Bahang, J.H., Park, H.L., Yoon, Y.S., and. Kim, J. K. (2002) Optical parameters in SnO_2 nanocrystalline textured films grown on p-InSb (111) substrates, Journal of Physics and Chemistry of Solids, 63, 881-885.

[6] Bhagwat, M., Shah, P., and Ramaswamy,V. (2003) Synthesis of nanocrystalline SnO_2 powder by amorphous citrate route, Materials Letters, 57, 1604-1611.

[7] Zhang, J., and Gao, L. (2004) Synthesis and characterization of nanocrystalline tin oxide by sol–gel method, Journal of Solid State Chemistry 177, 1425-1430.

[8] Farrukh, M.A., Heng, B.T., and Adnan, R. (2010) Surfactant-controlled aqueous synthesis of SnO_2 nanoparticles via the hydrothermal and conventional heating methods, Turk J Chemistry, 34,537-550.

[9] Li, Z., Shen, W., Zhang, X., Fang, L., andZu, X. (2008) Controllable growth of SnO_2 nanoparticles by citric acid assisted hydrothermal process, Colloids and Surfaces A: Physicochem. Eng. Aspects, 327, 17-20.

[10] Liu, Y., Yang, F., and Yang, X. (2008) Size-controlled synthesis and characterization of quantum-size SnO_2 nanocrystallites by a solvothermal route, Colloids and Surfaces A: Physicochem. Eng. Aspects, 312, 219-225.

[11] Pal, J., and Chauhan, P. (2009) Structural and optical characterization of tin dioxide nanoparticles prepared by a surfactant mediated method, Materials Characterization 60, 1512- 1516.

[12] Billik, P., and Čaplovičová, M. (2009) Synthesis of nanocrystalline SnO_2 powder from $SnCl_4$ by mechanochemical processing, Powder Technology,191, 235-239.

[13] Song, K.C., and Kim, J. H. (1999) Preparation of Nanosize Tin Oxide Particles from Water-in-Oil Microemulsions, Journal of Colloid and Interface Science, 212, 193-169.

[14] Gaber, A., Abdel- Rahim, M.A., Abdel-Latief, A.Y., and Mahmoud. N. Abdel-Salam. (2014) Influence of Calcination Temperature on the Structure and Porosity of Nanocrystalline SnO_2 Synthesized by a Conventional Precipitation method, Int. J. Electrochem. Sci., 9, 81-95.

[15] Gaber, A., Abdel- Rahim, M.A., Abdel-Latief, A.Y., and Mahmoud. N. Abdel-Salam. (2013) Thermally induced structural changes and optical properties of tin dioxide nanoparticles synthesized by a conventional precipitation method, Materials Science in Semiconductor Processing 16, 1784-1790.

[16] Song, K.C., and Kang, Y. (2000) Preparation of high surface area tin oxide powders by a homogeneous precipitation method, Materials Letters, 42, 283-289.

[17] Acarbas, Ö., Suvacı, E., and Dog˘an, A. (2007) Preparation of nanosized tin oxide (SnO_2) powder by homogeneous precipitation, Ceramics International, 33, 537-542.

[18] Djuriçić, B., Pickering, S., McGarry, D., Glaude, P., Tambuyser, R., and Schuster, K. (1995) The Properties of Zirconia Powders Produced by Homogeneous Precipitation, Ceramics International 21, 195-206.

[19] Toledo-Antonio, J. A., Baez, R.G., Sebastian, P.J., and Vazquez, A. (2003) Thermal stability and structural deformation of rutile SnO_2 nanoparticles, Journal of Solid State Chemistry 174, 241-248.

[20] Dolzan, A.A., Fong, C., Kennedy, B. J., and Howard, C.J., (1997) Structural Studies of Rutile-Type Metal Dioxides, ICDD-Card, ActaCrystallogr. Dec. B: Struct. Sci. 53(3) 373-380.

[21] Yang, H., Zhang, X., Ao, W., and Qiu, G. (2004) Formation of $NiFe_2O_4$ nanoparticles by mechanochemical reaction, Materials Research Bulletin, 39, 833-837.

[22] Yang, H., Hu, Y., Tang, A., Jin, S., and Qiu, G. (2004) Synthesis of tin oxide nanoparticles by mechanochemical reaction, J. of Alloys and Compounds, 363, 276-279.

[23] Hasanzadeh-Tabrizi, S.A., Mazaheri, M., Aminzare, M.,Sadrnezhad, S.K. (2009). 2nd International Conference on Ultrafine Grained and Nanostructured Materials University College of Engineering, University of Tehran, Tehran, Iran. 14-15 Nov.

[24] Baik, N. S., Miura, N., and Yamazoe, N. (2000) Hydrothermally treated sol solution of tin oxide for thin-film gas sensor, Sensors and actuators B 63, 74 -79.

[25] Wakefield, G., Holland, E., Dosban, P.J., and Hutchison, J. L. (2001) Luminescence Properties of Nanocrystalline Y_2O_3:Eu, Advanced Materials 13, 1557-1560.

[26] Gregg, S.J., and Sing, K.S.W. (1982), Adsorption, surface area, and porosity. Academic Press, London, 2nd. Edn.

[27] He, G., Bhat,G., and Chen, Z. W., (2011) Annealing driven performance and optical effects in nanocrystalline SnO_2 thin films induced by pulsed delivery, Journal of Alloys and Compounds 509, 9513-9517.

[28] Gondal, M.A., Drmosh, Q.A., and Saleh, T.A. (2010) Preparation and characterization of SnO_2 nanoparticles using high power pulsed laser, Applied Surface Science 256, 7067-7070.

[29] Dutta, K., and De, S. K., (2007) Optical and nonlinear electrical properties of SnO_2–polyaniline nanocomposites, Materials Letters 61, 4967-4971.

[30] Beydoun, D., Amal, R., Low, G., and S. McEvoy, S. (1999) Role of Nanoparticles in Photocatalysis Journal of Nanoparticle Research 1, 439-458.

[31] Sing, K.S.W., Everette, D.H., Haul, R.A.W., Moscou, L., Pierotti, R. A., Rouquerol,J., and Siemieniewska, T. (1985) Reporting physisorption data for gas/solid systems with special reference to the determination of surface area and porosity, Pure and Appl. Chem.57, 603-619.

[32] Leofanti, G., Padovan, M., Tozzola, G., and Venturelli, B., (1998) Surface area and pore texture of catalysts, catalyst today 41, 207-219.

[33] Song, K. C., and Kim, J. H. (2000) Synthesis of high surface area tin oxide powders via water-in-oil microemulsions, Powder technology 107, 268-272.

[34] Sergent, N., Gélin, P., Périer- Camby, L., Praliaud, H., and Thomas, G. (2002) Preparation and characterization of high surface area stannic oxides: structural, textural and semiconducting properties, Sensors and Actuators B 84, 176-188.